The Role of Collateral Paths in Long-Range Diffusion of ³He in Lungs

Mark S. Conradi[1,2], **Dmitriy A. Yablonskiy**[1,2], **Jason C. Woods**[1], **David S. Gierada**[2], **Seth-Emil T. Bartel**[1], **Susan E. Haywood**[1,2], and **Christopher Menard**[1]

1 *Washington University, Dept. Of Physics, Saint Louis MO 63130*

2 *Washington University, Dept, of Radiology, Saint Louis MO 63130*

Abstract

Rationale and Objectives—The hyperpolarized ³He long-range diffusion coefficient (LRDC) in lungs is sensitive to changes in lung structure due to emphysema, reflecting the increase in collateral paths resulting from tissue destruction. However, no clear understanding of LRDC in healthy lungs has emerged. Here we compare LRDC measured in healthy lungs with computer simulations of diffusion along the airway tree with no collateral connections.

Materials and Methods—Computer simulations of diffusion of spatially modulated spin magnetization were performed in computer generated, symmetric-branching models of lungs and compared with existing LRDC measurements in canine and human lungs.

Results—The simulations predict LRDC values of order 0.001 cm²/s, approximately 20 times smaller than the measured LRDC. We consider and rule out possible mechanisms for LRDC not included in the simulations: incomplete breath hold, cardiac motion, and passage of dissolved ³He through airway walls. However, a very low density of small (micron) holes in the airways is shown to account for the observed LRDC.

Conclusion—It is proposed that LRDC in healthy lungs is determined by small collateral pathways.

Keywords

Lung; diffusion MRI; gas MRI; restricted diffusion; long range diffusion; helium

Introduction

The advent of technology for the production of ~liter quantities of hyperpolarized ³He gas allows imaging of the air spaces of lungs. The first use of the technology was to produce ventilation images (1,2,3) which display the distribution of a single bolus of inhaled ³He at breath hold. Subsequently, dynamic ³He MRI was used to show the time evolution of gas distribution, with sub-second time resolution (4,5). A quantitative method for measurement of the local fractional ventilation (the fraction of gas replaced with each breath) has also appeared (6). The local oxygen concentration and its decrease during breath hold have been determined (7,8) from the ³He T_1, allowing the local ventilation – perfusion ratio to be calculated (9).

The microstructure of the lung (the acinar airways and alveolar walls) *restricts* the diffusion of ^{3}He. In emphysema, expansion of the acinar airways and tissue destruction result in less restriction and larger apparent diffusion coefficient (ADC). Measurements of the ADC are commonly performed (10–13) with two b-values, one of which is zero, with bipolar diffusion-sensitizing gradient pulses of 2–5 ms duration (here b is the weighting of the diffusion-sensitizing gradient pulses). For these times, the ^{3}He free diffusivity D_0 (in N_2 or air) of about 0.88 cm^2/s corresponds to rms displacements of about 0.7 mm, large enough to thoroughly explore the interior of a typical acinar airway. Measured ADC values in normal human lungs are approximately 0.2 cm^2/s and increase in emphysema; in severely diseased lungs, 0.6 cm^2/s is common (11). Likewise, increases of ADC in rats are observed in emphysema (12, 14). ^{3}He ADC measurements have yet to enter common clinical practice, though they are regarded as the emerging new gold-standard for characterizing the emphysema-component of COPD. Interest is high in using ^{3}He ADC for early detection of the disease and for following disease progression in drug treatment trials.

Based on existing knowledge of lung acinar structure, the acinar airways have been modeled (15) as long cylinders covered by a sleeve of alveoli. In these structures, diffusion is *anisotropic* with a large longitudinal value (D_L) and a smaller transverse value (D_T). The success of the model depends on (i) the *major radius* of all the acinar airways being nearly constant over the many airway-levels, and (ii) the diffusion time of the pulse sequence (~2ms) being short enough that most gas atoms remain in the same acinar airway throughout this time. This model has been used to analyze data to determine the mean acinar major radius in a normal volunteer, in excellent agreement (5%) with the value accepted from post-mortem measurements. Recent work (16) aims to obtain (primarily from D_L) the ratio of minor to major radii, which is a measure of the extent that alveoli enter into the acinar airways. The non-exponential signal decay can also be treated (17) in terms of a power-law expansion of the log of the signal in powers of b. The b^2 term (the curvature) can be expressed as the dimensionless kurtosis. The connection between the value of kurtosis and the lung microstructure is not clear, however.

The probability distribution of displacements, P(Δx), can be obtained as the Fourier transform of the signal amplitude with respect to the gradient amplitude. In lung, P(Δx) has been reported (18) to be approximately the sum of two Gaussians, one narrow and one wide. This is equivalent to writing the signal amplitude S(b) as the sum of two decaying exponentials (19).

Long-Range Diffusion

The ADC measurements discussed above use short diffusion times (milliseconds) and so allow the ^{3}He to explore individual acinar airways. Longer diffusion times (seconds) are required for the ^{3}He to explore longer distances, to reveal the *connectivity* of the airways and acini. Measurements of the long-range diffusion coefficient (LRDC) have appeared, using sinusoidal spatial modulation (20) of the ^{3}He spin magnetization, with modulation wavelengths λ of typically 2–3 cm (21–23). Diffusion occurring after the initial modulation (or tagging, or striping) reduces the amplitude of the modulation; small-angle (FLASH) imaging can follow the decaying amplitude and allow a LRDC value to be determined. By using the longitudinal spin magnetization, the decay due to diffusion can be followed to times of order T_1, the longest relaxation time in the spin system. Specifically, the modulated magnetization amplitude S will decay exponentially as (22)

$$S \sim \exp(-Rt), \text{where} \qquad [1]$$

$$R = (LRDC)k^2, \qquad [2]$$

and $k = 2\pi/\lambda$. The relevant diffusion distance is of order $\lambda/2$. The LRDC can also be measured with stimulated echo methods (24). The underlying physics is the same as the spatially modulated magnetization method, with the initial spin position encoded in the longitudinal magnetization. The primary difference between the methods is whether the modulation is done in the imaging plane or perpendicular to it. The stimulated echo method allows a wide range of modulation wavelengths and diffusion times to be explored (25).

The LRDC in healthy human volunteers (24,25) and healthy canines (22) has been measured to be about 0.02 cm^2/s using $\lambda = 2$ cm, approximately 10 times smaller than the 2 ms measurements of ADC. Similar values have been obtained (23) in explanted normal donor lungs (Figure 1). In emphysematous lungs, the LRDC increases substantially, by as much as a factor of 20 (Figure 2). There is evidence (23,26) that the ratiometric increase in LRDC (that is, the measured value divided by the normal value in health) is greater than the ratiometric increase of ADC (ms time scale). A very simplistic view is that restricted diffusivities cannot exceed the free diffusivity, D_0; as the normal LRDC is about $D_0/50$ and the normal ADC is about $D_0/5$, the LRDC has substantially "more room to grow", compared to the ADC.

In emphysema, the diffusion D_L along the acinar airways is likely to increase, because the interior of the expanded airways becomes smoother in relative terms (15); the alveolar walls no longer extend so far into the acinar airways. But this increase in D_L is limited to a factor of 2, since D_L in healthy lungs is approximately $D_0/2$ (15). So only a small part of the very large measured increases in LRDC can arise from the increased diffusivity along the airways. The diffusion transverse to the airways is completely unimportant as the acinar airway radii are much smaller than the relevant distance of $\lambda/2$. Thus, it is believed (22,23) that the measured increases in LRDC are due to increased *collateral paths*. Here, collateral paths are defined as all paths other than the canonical airway tree (27,28). The tissue destruction in emphysema increases the size and number of holes in the airway walls. These collateral paths represent short-circuits, allowing gas to diffuse between points which are nearby in space but are nevertheless quite distant along the airway tree (29). Thus, our current understanding is that LRDC is small in health because to travel between two points 1 cm apart (at least to another acinus), the gas must traverse the tortuous network of airways, finding the node on the airway tree which is common to the two points. With tissue destruction, this condition is greatly relaxed; there are many new, collateral routes between the two points.

But is it so? Is the LRDC in healthy lungs determined by gas diffusing only along the airway tree? Here, we report the results of computer simulations that indicate that LRDC in healthy lungs should be *much* smaller, if only paths along the airways proper are considered.

Computer Simulations

Healthy lungs were simulated according to the symmetric branching model of Weibel (29, 27); this model has 23 bifurcating levels of airways. In the model, airways are singly-connected, meaning any two points in the airway tree are linked by an unique path. The lengths and radii of the airways were taken from Table 1 of reference 29. Each parent airway gave birth to two daughters, at branching half-angle 40°. At each branch point, the plane of the daughters was rotated by a randomly chosen angle about the axis of the parent airway. The diffusion equation (30) in discrete form (not continuous) was solved for 32 random realizations of the structure, with randomly selected direction and phase of magnetization modulation. The modulation time-decay was fitted to the exponential decay of eqn. [1] and the decay rate constant R was used to determine the LRDC using eqn. [2]. The wavelength λ was set to 2 cm, in agreement with most existing experimental data; this is larger than the mean acinar linear dimension of 6 mm.

Details of the simulation are described elsewhere (31). Here we focus on the implications of the results.

Results

The simulated modulated magnetization decays (31) to nearly zero over a time interval of several hundred seconds. The decay is only approximately exponential; if one fits the time where the modulation has decayed by 1/e, one obtains a decay time constant (1/R) of about 115 s for $\lambda = 2$ cm. Using eqn [2], the LRDC in the simulation is thus about 0.001 cm^2/s. The 32 random versions of the simulated lung have similar time constants, with a 7% standard deviation. Variation of the branching half-angle from 35 to 45 degrees caused only ± 12% variation in the LRDC.

Discussion

The discrepancy between the simulated and measured LRDC values is extreme, with the measured LRDC 20 times larger. After the earliest measurements of LRDC, the question seemed to be "why is the LRDC so small compared to the ADC measured over milliseconds?" Now the question is "why is the measured LRDC so large?" We note that any routes additional to the airways proper, and so not taken into account in the simulations, could cause the observed discrepancy. We consider several possibilities below.

Lack of breath hold and cardiogenic mixing

Random (diffusive) rms displacements increase roughly as $\sqrt{t}$ while constant velocity motion results in displacement proportional to the diffusion time t (30). Thus, constant velocity motion, compared to diffusive motion, plays a relatively larger role at long diffusion times and long diffusion distances. Hence, motion of the heart and incomplete breath holds must be considered as potential sources of error for LRDC measurements. However, these sources cannot be present in the explanted lungs; we recall that LRDC measured *ex vivo* is also much larger than the simulation predictions (23). It is possible, of course, that these artifacts are weakly present *in vivo*.

Permeation through airway walls

What rate of overall, long-range diffusion results from the small permeability of ^{3}He through the airway walls? To estimate the diffusivity due to permeation, we model the lung in Figure 3 as a set of thin parallel membranes of thickness x and spaced by L-x; we assume L ≫ x. The membrane is primarily water (saline or blood), so the solubility of helium in water is used in the form of the Ostwald partition coefficient, s. That is, s is the ratio of ^{3}He concentration in the liquid to that in the gas at equilibrium. Using the same units for the two concentrations, the solubility s is dimensionless. For helium in water, the solubility s (32) is approximately 0.96 $\times 10^{-2}$. The ^{3}He residing in the membrane diffuses more slowly than in the gas; its diffusivity D_W in water may be estimated (33) as several times larger than the self-diffusion of water, thus no larger than 10^{-4} cm^2/s. The overall diffusivity LRDC can be derived by using Fick's law of diffusive flux,

$$J= - D\nabla C. \tag{3}$$

Here the flux is measured in particles (or spins) per time per area and C is in particles (or spins) per volume.

We consider the concentrations C at the specified points in Figure 3, over the length L of one period. The simple geometry of Figure 3 does not capture the details of the airway tree; this is of no concern, as the diffusion along the airways has already been considered in the simulations

and found to result in much smaller LRDC than the measured values. We assume that concentration equilibrium occurs along each gas-membrane interface and that the gas phase diffusion is infinitely rapid (more precisely, the diffusive bottleneck occurs in the membranes). Thus, the concentration variation across each gas-phase region is negligible. At steady-state, the flux from left to right in Figure 3 is the same across each membrane and airspace. Examining just the membrane, we write eqn. [3] above as

$$J = -D_w \frac{sC_2 - sC_1}{x}.$$ [4]

In terms of the structure of length L, we express the overall diffusivity LRDC using eqn. [3] in the same way,

$$J = -(LRDC)\frac{C_2 - C_1}{L}.$$ [5]

Equating the two expression for the flux J, we obtain

$$LRDC = D_w sL/x.$$ [6]

This result is correct when the LRDC so determined is much smaller than the gas free diffusion, D_0. Using the above values of D_W and s and setting L = 600 μm and x = 6 μm, reasonable estimates for acinar airways (27), we obtain LRDC = 10^{-4} cm^2/s. This is *much* smaller than the observed values of LRDC and even much smaller than the computer simulated results. We note that the gas-phase diffusivity is not infinite, which will make the overall diffusivity LRDC only (slightly) smaller. In the same way, lack of equilibrium of the concentration at the gas-liquid surfaces will also reduce LRDC. Overall, the diffusion through the structure of Figure 3 can be regarded as several processes in series, so the overall diffusivity is no larger than the result of eqn. [6]. We conclude that this mechanism is negligible, as a result of the low solubility of ^{3}He in water and its slow diffusion in water. We note that eqn. [6] was derived using a linear concentration (or spin magnetization) variation along x, but the result is fully general for length scales longer than L.

The above mechanism can be enhanced by the flow of blood in the capillary bed. Thus, ^{3}He can dissolve through the airway walls and into the blood and then be swept to distant locations. The process is completed by ^{3}He returning to the air space. In any event, this mechanism is certainly not applicable to the results for *ex vivo* lungs and so it can not explain the discrepancy of measured and simulated LRDC.

Diffusion through holes

Next we consider diffusion through isolated small holes in the walls of Figure 3. Again, we approach the problem by calculating the diffusive flux with Fick's law, eqn. [3]. As in Figure 4, consider each wall of area A to have a single hole of radius r; the concentrations on the two sides of the wall are C_1 and C_2, far from the hole. The concentration in each region will be essentially constant, except within a distance of about r from the hole. Thus, the concentration is expected to vary from C_1 to C_2 along the dashed line path of length 2r passing through the center of the hole in Figure 4. The diffusive flux J from eqn. [3] times the area πr^2 is the diffusive current I,

$$I = D_o \frac{C_2 - C_1}{2r}\pi r^2 = D_o(C_2 - C_1)r\pi/2;$$ [7]

here, D_0 is the free diffusivity of the gas. This result, aside from the numerical factor (which is only approximate), can be obtained by dimensional analysis.

A proper treatment of the problem involves the steady-state solution of the diffusion equation, $\nabla^2 c = 0$ where c is concentration (spin magnetization). It turns out that this is exactly analogous to the problem of finding the electrical conductance of the single short throat of radius r connecting two large regions, all with conductivity σ. This result is current

$$\text{Conductance} = \frac{\text{current}}{\text{potential difference}} = 2\sigma r. \tag{8}$$

This result is obtainable from the electrostatic capacitance CA of a conducting disk relative to a (grounded) surrounding conductor at infinity. The result is given by Smythe (34) as CA = $8\varepsilon_0 r$, where ε_0 is the permittivity of free space. Thus, the capacitance to top or bottom alone is $4\varepsilon_0 r$; the electrostatic and electrical conduction equations are analogous upon substituting the electrostatic ε_0 for the electrical conductivity σ. We note that the two electrical conductances of $4\sigma r$ in series form a single, net conductance of $2\sigma r$. In terms of diffusion, the diffusive conductance of the hole is therefore correctly given by

$$\text{conductance} = \frac{I}{C_2 - C_1} = 2D_0 r, \tag{9}$$

which differs numerically only slightly from the simple estimate of eqn. [7]. This result has been confirmed by numerical solution of $\nabla^2 c = 0$. The result also appears in Berg (35).

Considering a wall with N well-separated holes per area A, the overall flux J, averaged over the area of the wall, will be

$$\bar{J} = \frac{\text{current}}{A} = \frac{N}{A} 2D_0 r(C_2 - C_1). \tag{10}$$

Viewed overall, J can be expressed in terms of the overall diffusivity LRDC and the overall concentration gradient $(C_2-C_1)/L$,

$$\bar{J} = LRDC(C_2 - C_1)/L, \tag{11}$$

giving

$$LRDC = 2nD_0 rL, \tag{12}$$

where n is the number density of holes, n=N/A.

We note that a remarkably small density of small holes can account for the measured values of LRDC. For example, for holes of radius r = 5 μm = 5×10^{-3} mm (consistent with what is known of pores of Kohn (28,36)) and wall spacing L=600 μm, the hole density must be n=330 holes/cm^2 to account for the observed LRDC/$D_0 \cong$ 1/50. For a regular square pattern of holes, this is a hole spacing of 0.55 mm, of order one hole in each alveolar wall. If each hole is larger, then an even smaller density of holes is required. The fraction F of wall that must be hole to explain the observed LRDC is surprisingly small. In the above example, the fraction is F=$n\pi r^2$=2.6×10^{-4}. We note that, because of the linear (not quadratic) dependence of LRDC upon r, the fraction F will depend on the hole radius r, for given values of LRDC/D_0 and L.

The calculated LRDC of such a small density of very small holes suggests that these collateral paths may explain the factor of 20 discrepancy between the simulated and measured long-range

diffusivities. However, we do not intend the above numerical values of hole density and radius to be taken as measurements or facts, but only as estimates that are certainly in accord with what is known about collateral paths. That is, such a density and radius of holes is plausible. We note that other passages, those of Lambert and Martin, have been discussed (28).

It is a well known result that the collateral airflow resistance (37–42) is much larger than the airway resistance in normal human lungs. Thus, it is at first surprising that the long-range diffusion through collateral paths appears to be more important than the diffusion along the airway tree itself. However, we note two important differences. First, the collateral airflow resistances have been measured using the wedged catheter technique, typically at the level of individual lobes, segments, or sub-segments (28,38,42) (certainly in the conductive zone). The diffusive paths discussed above are presumably at a level to connect one acinus to its neighbor, so the relevant collateral paths are at a much lower level in the lung (in the diffusive zone). Second, the measured resistances involve hydrodynamic flow; we recall that laminar flow in a tube of radius r varies as r^4, for a fixed pressure differential and length (43). By comparison, the diffusive transport is proportional to r^2 (note the difference here with the case of a hole of no length, eqn. [7]).

Thus, a set of very small holes may offer a high resistance to transport by flow yet serve as an important path for diffusion. The fundamental distinction is that hydrodynamic flow resistance occurs at the cylinder wall while diffusion encounters resistance across the entire cross-section.

A recent calculation of diffusion within single acini has appeared (44), suggesting that the results explain the LRDC in healthy lungs. We note that the length scale is not specified, but can be no larger than the linear size of acini, about 6 mm. Because this is smaller than the striping wavelength, complete diffusion randomization within each acinus can only slightly reduce the stripe amplitude, from unity to approximately 0.75 for $\lambda = 2$ cm (31). Thus, intra-acinar diffusion can not explain the decay of stripes with $\lambda = 2$ cm and longer.

Conclusions

Long range diffusion (LRDC) measurements involve modulation of ^{3}He longitudinal spin magnetization with wavelengths of 2 or 3 cm. Values near 0.02 cm^2/s have been determined previously *in vivo* in normal dogs (22) and human volunteers (21) as well as *ex vivo* in normal human donor lungs (23). These values are similar to those measured using the stimulated echo method (24,25). Computer simulations of the diffusive decay of modulated magnetization have been performed in symmetric-branching model lungs. The simulations predict LRDC values approximately 20 times smaller than the measured values. Several possible sources of the large discrepancy are examined and ruled out: cardiac motion, incomplete breath hold, and diffusion of ^{3}He through the airway walls by dissolving into the membranes. However, consideration of the diffusion through a single hole shows it is proportional to the radius (not radius-squared). We calculate that a remarkably small density of small holes in the airway walls can account for the observed LRDC. For the numerical values used, n = 330 hole/cm^2 and r = 5 μm, the fraction of each wall that must be hole is less than 0.03%. We conclude that collateral paths may determine the LRDC in healthy lungs, just as they are believed to be responsible for the greatly enhanced LRDC values found in emphysematous lungs.

References

1. Möller HE, Chen XJ, Saam B, Hagspiel KD, Johnson GA, Altes TA, de Lange EE, Kauczor H-U. MRI of the lungs using hyperpolarized noble gases. Magn Reson Med 2002;47:1029–1051. [PubMed: 12111949]

2. Leawoods JC, Yablonskiy DA, Saam BT, Gierada DS, Conradi MS. Hyperpolarized [3]He gas MR imaging. Concepts Magn Reson 2001;13:277–293.

3. Hoffman EA, van Beek E. Hyperpolarized media MR imaging – Expanding the boundaries? Acad Rad 2006;13:929–931.

4. Saam BT, Yablonskiy DA, Gierada DS, Conradi MS. Rapid imaging of hyperpolarized gas using EPI. Magn Reson Med 1999;42:507–514. [PubMed: 10467295]

5. Salerno M, Altes TA, Brookeman JR, de Lange EE, Mugler JP III. Dynamic spiral MRI of pulmonary gas flow using hyperpolarized [3]He: preliminary studies in healthy and diseased lungs. Magn Reson Med 2001;46:667–677. [PubMed: 11590642]

6. Deninger AJ, Mansson S, Petersson JS, et al. Quantitative measurement of regional lung ventilation using [3]He MRI. Magn Reson Med 2002;48:223–232. [PubMed: 12210930]

7. Deninger AJ, Eberle B, Ebert M, et al. Quantification of regional intrapulmonary oxygen partial pressure evolution during apnea by [3]He MRI. J Magn Reson 1999;141:207–216. [PubMed: 10579944]

8. Fischer MC, Kadlecek S, Yu JS, Ishii M, Emami K, Vahdat V, Lipson DA, Rizi RR. Measurements of regional alveolar oxygen pressure using hyperpolarized He-3 MRI. Acad Rad 2005;12:1430–1439.

9. Rizi RR, Baumgardner JE, Ishii M, et al. Determination of regional VA/Q by hyperpolarized [3]He MRI. Magn Reson Med 2004;52:65–72. [PubMed: 15236368]

10. Salerno M, de Lange EE, Altes TA, Truwit JD, Brookeman JR, Mugler JP. Emphysema: hyperpolarized helium 3 diffusion MR imaging of the lungs compared with spirometric indexes – initial experience. Radiology 2002;222:252–260. [PubMed: 11756734]

11. Saam BT, Yablonskiy DA, Kodibagkar VD, Leawoods JC, Gierada DS, Cooper JD, Lefrak SS, Conradi MS. MR imaging of diffusion of He-3 gas in healthy and diseased lungs. Magn Reson Medicine 2000;44:174–179.

12. Chen XJ, Hedlund LW, Möller HE, Chawla S, Maronpot RR, Johnson GA. Detection of emphysema in rat lungs by using magnetic resonance measurements of [3]He diffusion. Proc Natl Acad Sci USA 2000;97:11478–11481. [PubMed: 11027348]

13. Conradi MS, Yablonskiy DA, Woods JC, Gierada DS, Jacob RE, Chang YV, Choong CK, Sukstanskii AL, Tanoli T, Lefrak SS, Cooper JD. [3]He diffusion MRI of the lung. Acad Rad 2005;12:1406–1413.

14. Peces-Barba G, Ruiz-Cabello J, Cremillieux Y, et al. Helium-3 MRI diffusion coefficient: correlation to morphometry in a model of mild emphysema. Eur Respir J 2003;22:14–19. [PubMed: 12882445]

15. Yablonskiy DA, Sukstanskii AL, Leawoods JC, Gierada DS, Bretthorst GS, Lefrak SS, Cooper JD, Conradi MS. Quantitative *in vivo* assessment of lung microstructure at the alveolar level with hyperpolarized [3]He diffusion MRI. Proceeding National Academy of Sciences 2002;99:3111–3116.

16. Sukstanskii AL, Conradi MS, Yablonskiy DA. Relationship between [3]He gas ADCs and lung microstructure. Computer simulations. Proc Intl Soc Magn Reson Med 2007;15:1335.

17. Jensen JH, Helpern JA, Ramani A, Hanzhang L, Kaczynski K. Diffusion kurtosis imaging: the quantification of non-Gaussian water diffusion by means of magnetic resonance imaging. Magn Reson Med 2005;53:1432–1440. [PubMed: 15906300]

18. Shanbhag DD, Altes TA, Miller GW, Mata JF, Knight-Scott J. Q-space analysis of lung morphmetry in vivo with hyperpolarized [3]He spectroscopy. J Magn Reson Imag 2006;24:84–94.

19. Shanbhag DD, Altes TA, Mata JF, Miller GW, Knight-Scott J. SNR performance of Q-space formalism and multi-exponential modeling for hyperpolarized [3]He gas diffusion spectroscopy in human lungs. Proc Intl Soc Magn Reson Med 2007;15:1286.

20. Alex L, Dougherty L. MR imaging of motion with spatial modulation of magnetization. Radiology 1989;171:841–845. [PubMed: 2717762]

21. Owers-Bradley, JR.; Bennattayalah, A.; Fichele, S.; McGloin, JC.; Bowtell, R.; Morgan, PS.; Moody, AR. Diffusion and tagging of hyperpolarized [3]He in the lungs. Proc 10th Annual Meeting International Society for Magnetic Resonance in Medicine; Honolulu, Hawaii. 2002. p. 2016

22. Woods JC, Yablonskiy DA, Chino K, Tanoli TSK, Cooper JD, Conradi MS. Magnetization tagging decay to measure long-range ^{3}He diffusion in healthy and emphysematous canine lungs. Magn Reson Med 2004;51:1002–1008. [PubMed: 15122683]

23. Woods JC, Choong CK, Yablonskiy DA, Chino K, Macklem PT, Pierce JA, Cooper JD, Conradi MS. Long-range diffusion of hyperpolarized ^{3}He in excised normal and emphysematous human lungs via magnetization tagging. J Appl Physiology 2005;99:1992–1997.

24. Wang C, Miller GW, Altes TA, de Lange EE, Cates GD Jr, Mugler JP III. Time dependence of ^{3}He diffusion in the human lung: measurement in the long-time regime using stimulated echoes. Magn Reson Med 2006;56:296–309. [PubMed: 16791861]

25. Wang C, Miller GW, Altes TA, de Lange EE, Brookeman JR, Cates GD Jr, Mugler JP III. Measuring medium and long-time-scale regional ^{3}He diffusion using stimulated echoes. Proc Intl Soc Magn Reson Med 2007;15:458.

26. Wang C, Altes TA, Miller GW, de Lange EE, Ruppert K, Brookeman JR, Mata JF, Cates GD Jr, Mugler JP III. Short-time-scale and long-time-scale ^{3}He diffusion MRI in emphysema: which is more sensitive? Proc Intl Soc Magn Reson Med 2007;15:941.

27. West, JB. Respiratory physiology. 5. Baltimore, MD: Williams & Wilkins; 1995. p. 21-30.

28. Menkes, HA.; Macklem, PT. Collateral flow. In Handbook of physiology, section 3: The respiratory system. Fishman, AP., editor. Bethesda MD: Amer Physiological Society; 1977. p. 337-353.

29. Weibel, ER. Design of airways and blood vessels considered as branching trees. In: Crystal, RG.; West, JB.; Barnes, PJ.; Weibel, ER., editors. The lung: scientific foundations. 2. Philadelphia: Lippencott-Raven; 1997. p. 1061-1071.

30. Mathews, J.; Walker, RL. Mathematical methods of physics. Menlo Park, CA: WA Benjamin; 1970. p. 217-252.

31. Bartel SET, Haywood SE, Woods JC, Chang YV, Menard C, Yablonskiy DA, Gierada DS, Conradi MS. Simulations and measurements of long-range diffusion of gas in lungs. In preparation

32. Lide, DR., editor. CRC handbook of chemistry and physics. 85. Boca Raton. FL: CRC Press; 2004. p. 8-87.

33. Kirchner B, Stubbs J, Marx D. Fast anomalous diffusion of small hydrophobic species in water. Phys Rev Lett 2002;89:215901–215904. [PubMed: 12443432]

34. Smythe, WR. Static and dynamic electricity. New York, NY: McGraw-Hill; 1968. p. 124

35. Berg, HC. Random walks in biology. Princeton NJ: Princeton U; 1993.

36. Bastacky J, Goerke J. Pores of Kohn are filled in normal lungs: low-temperature scanning electron microscopy. J Appl Physiol 1992;73:88–95. [PubMed: 1506404]

37. Woolcock AJ, Macklem PT. Mechanical factors influencing collateral ventilation in human, dog and pig lungs. J Appl Physiol 1971;30:99–115. [PubMed: 5538799]

38. Terry PB, Traystman RJ, Newball HH, Batra G, Menkes HA. Collateral ventilation in man. New Engl J Med 1978;298:10–15. [PubMed: 618444]

39. Hogg JC, Macklem PT, Thurlbeck WM. The resistance of collateral channels in excised human lungs. J Clin Invest 1969;48:421–431. [PubMed: 5773080]

40. Macklem PT. Collateral ventilation. New Engl J Med 1978;298:49–50. [PubMed: 618452]

41. Cetti EJ, Moore AJ, Geddes GM. Collateral ventilation. Thorax 2006;61:371–373. [PubMed: 16648350]

42. Inners CR, Terry PB, Traystman RJ, Menkes HA. Effects of lung volume on collateral and airway resistance in man. J Appl Physiol 1979;46:67–73. [PubMed: 457532]

43. Kundu, PK.; Cohen, IM. Fluid mechanics. 2. New York: Academic; 2002.

44. Verbanck S, Paiva M. Simulation of the apparent diffusion of helium-3 in the human acinus. J Appl Physiol 2007;103:249–254. [PubMed: 17379747]
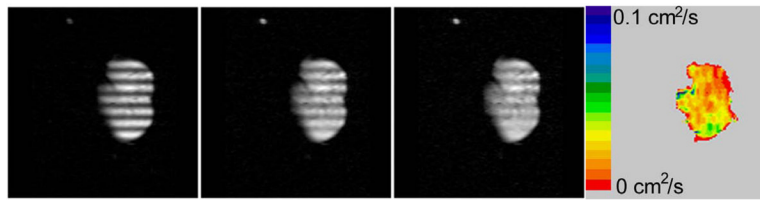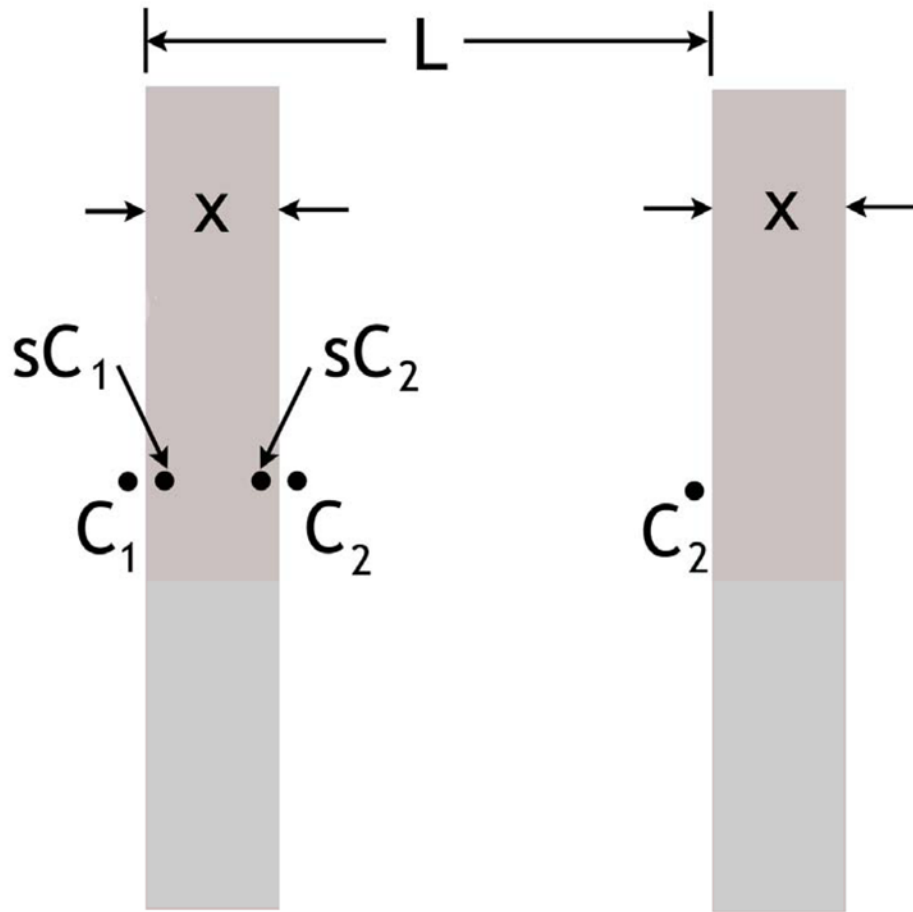
Figure 1.
Modulated magnetization images in an explanted normal donor lung at times of 0, 2, and 4 s (frames 1–3) after modulation. The long-range diffusivity LRDC appears in color. The striping wavelength λ is 2 cm in this axial, 30 mm slice with 450 mm field of view and 128×128 in-plane matrix.
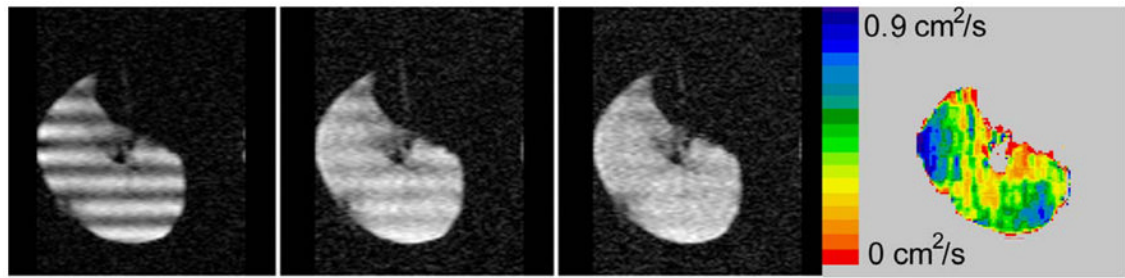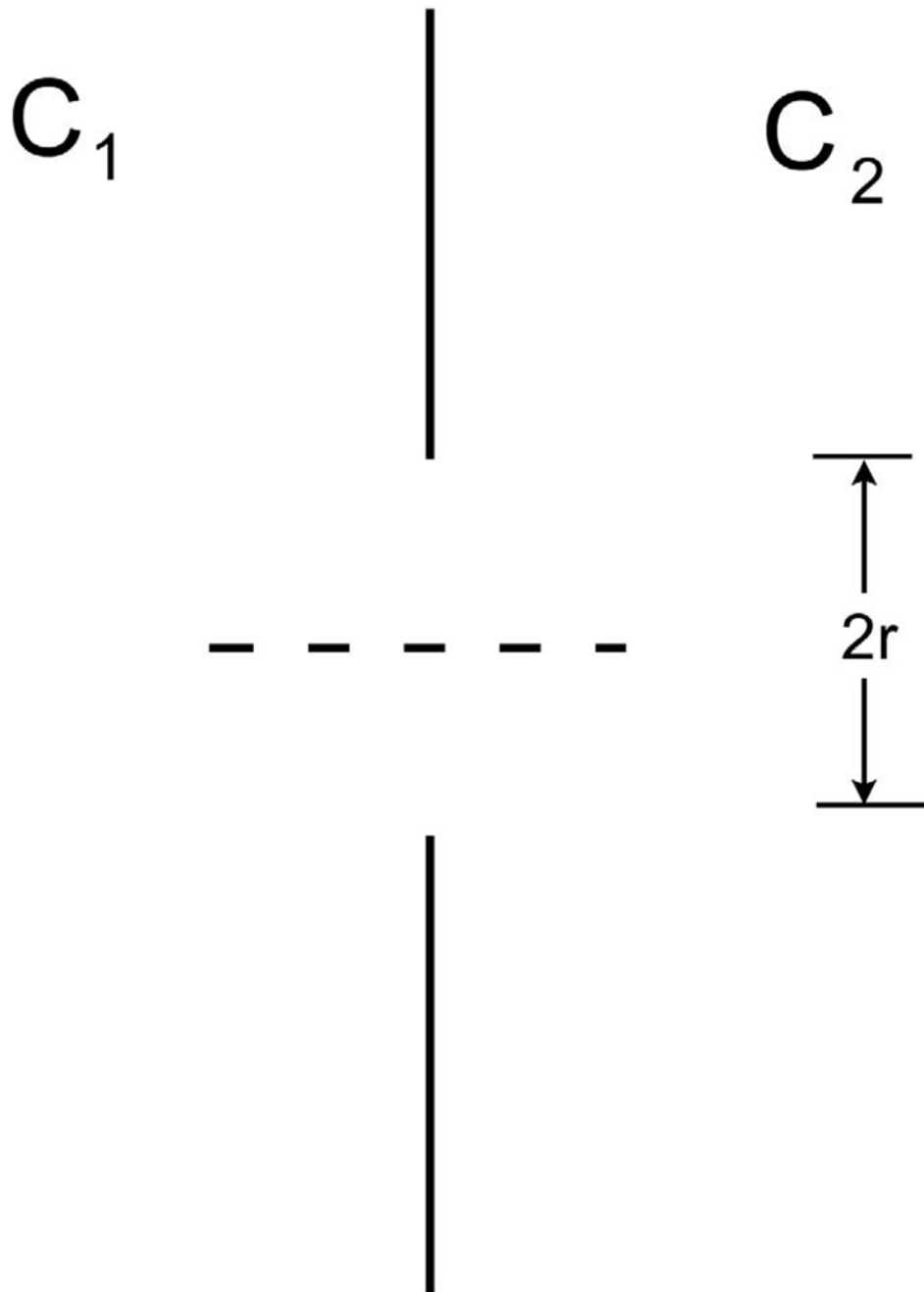
Figure 2.
Modulated magnetization images of an explanted lung with COPD stage GOLD-IV. Frames 1–3 are at times of 0, 0.6, and 1.2 s. Note the much larger color scale here for LRDC than in Figure 1. Here λ is 3 cm in this approximately axial slice of 30 mm thickness, field of view of 350 mm and 128×128 in-plane matrix.

Figure 3.
Periodic structure of length L of thin walls used to model effect of diffusion through lung airway walls. The concentrations C are shown at the relevant locations, spanning one unit of the periodic structure. The dimensionless solubility is s. The walls extend indefinitely in the vertical direction and perpendicular to the page.

Figure 4.
Wall of area A with a single hole of radius r. Along the path of the dashed line, the concentration changes by approximately $C_1 - C_2$ in distance 2r.